

Phase space dynamics of triaxial collapse: I. Joint density-velocity evolution

Sharvari Nadkarni-Ghosh^{1*} and Akshat Singhal^{2†}

¹*Department of Physics, I.I.T. Kanpur, Kanpur, U.P. 208016 India*

²*Department of Mathematics and Statistics, I.I.T. Kanpur, Kanpur, U.P. 208016 India*

ABSTRACT

We investigate the dynamics of triaxial collapse (in the absence of rotations) in terms of a new set of nine *dimensionless variables*. These nine variables correspond to the eigenvalues of the deformation tensor (λ_a), the tensor of velocity derivatives (λ_v) and the Hessian of the gravitational potential (λ_d). Starting from the well-known equations of Bond & Myers, we derive a new set of evolution equations for the nine eigenvalues and examine their dynamics in phase space. The main advantage of this form is that it eliminates the complicated elliptic integrals that appear in the axes evolution equations and is a more natural way to understand the interplay between the perturbations.

This paper, the first in a series of two, focuses on the density-velocity dynamics. In the linear regime, the Zel’dovich approximation implies that the three tensors are proportional; the proportionality constant is set by demanding ‘no decaying modes’. This relation is extended into the non-linear regime by imposing the condition ‘no perturbations at the big bang epoch’. This gives an implicit relation between the three λ_d and λ_v tracing out a special plane in the 6D phase space, which we call the ‘Zel’dovich hyperplane’. We show that at late times all density and velocity fluctuations lie on this plane to an accuracy of 1%. It is often assumed that, in the ‘linear’ regime, the fractional density contrast δ is equal to the sum of the eigenvalues of the deformation tensor. We analyse the validity of this approximation and find that it strictly holds true only for very early epochs. At later epochs, due to the triaxiality, the relation breaks down even for linear values of δ . Finally, we examine the dynamics in the 2D density-velocity divergence phase space and discuss the relation between the scatter and the shear component of the velocity field. As an application, we numerically compute the one point PDFs of the two variables and compare to some existing forms in the literature. We find that this simple model is able to reproduce the behaviour in voids rather well, but disagrees at high densities.

Key words: cosmology: large-scale structure of Universe

1 INTRODUCTION

Modeling the non-linear growth of fluctuations and in particular understanding the relation between the density and velocity sectors is an important issue in cosmology today. Although numerical simulations are becoming increasingly efficient, the need for analytic approaches still remains. Perturbative methods are extremely useful, but have limited validity and extending them to the non-linear regime requires sophisticated resummation techniques (see for e.g., Matsubara 2008; Matarrese & Pietroni 2007; Nadkarni-Ghosh & Chernoff 2011, 2013). However, restricting the dynamics to simpler geometries can sometimes give considerable insights into the non-linear regime. The simplest of such models is the spherical top-hat model (Gunn & Gott 1972; Peebles 1980). The main attractive feature of this model is that analytic solutions can be obtained for pure matter dominated cosmologies. But observed luminous galaxies or clusters and the simulated dark matter haloes (for e.g. Jing &

* E-mail: sharvari@iitk.ac.in

† E-mail: akshat.singhal014@gmail.com

Suto 2002) are more ellipsoidal than spherical and hence a more realistic description of the dynamics is given by assuming an ellipsoidal or triaxial geometry. The problem of gravitational collapse of a homogenous ellipsoid has been studied to various levels of approximations since the 1960s. Early studies (Lynden-Bell 1964; Lin, Mestel, & Shu 1965) examined the isolated ellipsoid in a non-expanding background. Cosmological extensions were performed by Icke (1973) and White & Silk (1979) but under the assumption that the background did not exert an external forces on the ellipsoid. Bond & Myers 1996 (hereafter BM96) included the effect of the background in terms of an external tidal field and a recent extension to their model was provided by Angrick & Bartelmann (2010). Eisenstein & Loeb (1995) provided a more complete analytic model that includes rotation as well.

Both spherical and triaxial collapse models are local in the sense that the dynamics of the perturbation variables at a given point depends only the initial values of the variables at that point. Although the full dynamics is non-local (i.e., the gravitational field needs to be known everywhere), such local approximations have proven to be extremely useful. For example, Press & Schechter (1974) first used the critical density for collapse predicted by spherical dynamics as important ingredient in constructing the mass function. Later, extensions were performed using ellipsoidal dynamics (for e.g., Monaco 1995; Sheth, Mo, & Tormen 2001). Other applications include predicting the non-linear probability distribution function (PDF) of density and velocity fields (Fosalba & Gaztanaga 1998b,a; Scherrer & Gaztanaga 2001; Ohta, Kayo, & Taruya 2003, 2004; Lam & Sheth 2008b,a), predicting collapse times for halo formation (Monaco et al. 2013) or building haloes from dark matter simulations (Despali, Tormen, & Sheth 2013). In many of these applications the ellipsoidal model performs better than the spherical one.

Recently, Bilicki & Chodorowski (2008) used the spherical top-hat model to derive an analytic form for the non-linear relation between density (δ) and the (scaled) velocity divergence (Θ). They showed that it slightly improved the analytic form given by Bernardeau (1992) based on perturbation theory. Nadkarni-Ghosh (2013) (hereafter N13) generalized their result by examining the dynamics of spherical perturbations in the joint 2D $\delta - \Theta^1$ phase space. This method did not depend on any analytic solutions of the top-hat. Instead it extended the requirement of ‘no decaying modes’ used in the linear solution to the non-linear regime. This analysis showed that the condition ‘no perturbations at the big bang’ can be imposed at any epoch to give a non-linear relation between the density and the velocity divergence. The relation traces out a special curve in phase space which was termed ‘Zel’dovich curve’. The Zel’dovich curve turns out to be an ‘attracting’ solution i.e., small initial perturbations starting anywhere in phase space are eventually attracted to this curve and those that start along it stay along it to a high degree of accuracy. This curve was examined for a range of flat dark energy cosmologies with constant equation of state. It was found that a combination of the analytic forms of Bilicki & Chodorowski (2008) and Bernardeau (1992), extended to include the dark energy dependence, provided a good fit to the Zel’dovich curve.

In this paper, our aim is to examine triaxial collapse from a similar phase space point of view. Instead of two dimensionless variables δ and Θ , the triaxial system needs six. We identify these as the three eigenvalues (λ_d) of the Hessian (tensor of second partial derivatives) of the peculiar gravitational potential and three eigenvalues (λ_v) of the tensor of partial derivatives of the velocity field ². The trace of the former is δ and that of the latter is Θ . The Zel’dovich curve now becomes a relation between these six variables which we refer to as the ‘Zel’dovich’ hyperplane. Since the internal potential of the triaxial system is intimately connected to its shape, these six variables are connected to the three eigenvalues of the deformation tensor (λ_a). Starting from the BM96 set of equations for triaxial collapse, we obtain a set of nine coupled one-dimensional equations governing the dynamics of these eigenvalues. This new set is more advantageous to work with because it eliminates the need for the elliptic integrals that appear in the original evolution equations for axes lengths. Using this set, we demonstrate that the Zel’dovich hyperplane to an accuracy of 1% acts like an attracting subspace in the 6D phase space. The hyperplane being a higher dimensional object cannot be directly visualized; instead we plot 2D subspaces to see the relation between the density and velocity variables for each axis. This analysis also gives us insight into the relation between the density and the trace of the deformation tensor ($\sum \lambda_i$). It is usually assumed that the linear regime, which usually refers to ‘small’ density contrasts, these are the same. We illustrate that for this to be true, it does not suffice for the density to be small; the individual eigenvalues of the gravitational shear tensor should be small. At later epochs, it is erroneous to equate the trace of the deformation tensor to the density, even when the density is small.

In order to understand the non-linear density-velocity relation we examine the dynamics in the 2D $\delta - \Theta$ space. We find that the relation has a scatter with the Zel’dovich curve forming an upper bound. We show that this scatter can be attributed to the (traceless) ‘shear’ part of the velocity field. Chodorowski (1997) discussed this point based on perturbation theory, the ellipsoidal collapse provides an alternate view of the same based on ‘local dynamics’. Finally, as an application we numerically compute the marginal one-point PDFs of the density and velocity divergence and compare them to some existing forms in the literature. The analysis of the evolution of the deformation tensor and the resulting axis ratios is the subject of a subsequent paper (paper II; Nadkarni-Ghosh & Singhal; in preparation).

The paper is organised as follows. §2 establishes the notation and the equations for the nine eigenvalues starting from

¹ In N13, we used θ instead of Θ .

² These two are often referred to as ‘gravitational shear’ and ‘velocity shear’ tensors respectively. However, we will keep this terminology only for the traceless part of these tensors.

the well known equations for axes evolution (BM96). The computational definition of the ‘Zel’dovich hyperplane’ is discussed and its relevance in the phase space evolution is demonstrated. §3 discusses the dynamics in the 2D $\delta - \Theta$ plane. Differences with the spherical case are discussed and the origin of the scatter is analysed. §4 derives the one point PDFs numerically and compares it to existing forms in the literature. §5 provides a summary and conclusion. Throughout this paper the terms ‘ellipsoidal’ and ‘triaxial’ are used interchangeably.

2 DYNAMICS OF THE ELLIPSOID

2.1 Notation and equations

Consider a uniform ellipsoidal distribution of cosmological fluid consisting of dark matter and dark energy evolving in a flat, homogenous and isotropic background. Let $\rho_{m,e}$ be the matter density inside the ellipsoid. It differs from the background matter density $\bar{\rho}_m$; the difference is characterized by the fractional density $\delta = \rho_{m,e}/\bar{\rho}_m - 1$. The dark energy is the same inside and outside the ellipsoid and is described by a cosmological constant with density ρ_Λ . Let the origin be at the centre of the ellipsoid. The ellipsoid can be completely characterized by the evolution of its three principal axes. In this paper we follow the equations of BM96, which assume that the direction of the axes remains unchanged throughout the evolution. The physical coordinate of each axis r_i can be written as $r_i = a_i(t)q$ ($i = 1, 2, 3$), where q is the comoving radius of the corresponding ‘Lagrangian sphere’ (BM96): this is a sphere concentric with the ellipsoid whose mass equals that of the ellipsoid but whose density is the same as the background. a_i are the ‘scale factors’ of each axis and a is the background scale factor. Throughout this paper we will use the subscript ‘ i ’ to index the axes and ‘ $init$ ’ to denote initial conditions. Mass conservation during evolution implies $a^3 q^3 \bar{\rho}_m = a_1 a_2 a_3 q^3 \rho_{m,e}$ giving

$$\delta = \frac{a^3}{a_1 a_2 a_3} - 1. \quad (1)$$

The evolution of a_i according to BM96 is ³

$$\frac{d^2 a_i}{dt^2} = -4\pi G \left[\frac{\bar{\rho}_m}{3} - \frac{2}{3} \rho_\Lambda \right] a_i - 4\pi G \left[\bar{\rho}_m \left\{ \frac{\delta \alpha_i}{2} + \lambda_{ext,i} \right\} \right] a_i, \quad (2)$$

where

$$\alpha_i = a_1 a_2 a_3 \int_0^\infty \frac{d\tau}{(a_i^2 + \tau) \prod_{j=1}^{j=3} (a_j^2 + \tau)^{1/2}} \quad \text{with} \quad \left(\sum_{i=1}^3 \alpha_i = 2 \right) \quad (3)$$

$$\lambda_{ext,i} = \frac{5}{4} \left(\alpha_i - \frac{2}{3} \right) \quad \text{non-linear approx.} \quad (4)$$

In eq. (2), the first term in square brackets corresponds to the background potential and the second term to the perturbation potential. The α_i s are parameters that describe the internal potential of the ellipsoid and are computed using Carlson’s elliptic integrals (Carlson 1987, 1989; Press et al. 2002; see appendix B for relations). $\lambda_{ext,i}(t)$ models the external tidal field. In this paper, we will use the non-linear approximation ⁴. Using standard definitions: $\bar{\rho}_m = \Omega_m \rho_c$, $\rho_\Lambda = \Omega_\Lambda \rho_c$ and $H^2 = 8\pi G \rho_c / 3$ and converting the time variable to a gives

$$\frac{d^2 a_i}{da^2} + \left\{ \frac{1}{Ha} \frac{d}{da} (Ha) \right\} \cdot \frac{da_i}{da} = -\frac{3}{2a^2} \left[\Omega_m(a) \left(\frac{1}{3} + \frac{\delta \alpha_i}{2} + \lambda_{ext,i} \right) - \frac{2}{3} \Omega_\Lambda(a) \right] a_i. \quad (5)$$

Note that the Ω parameters are functions of a and are related to their values today ($a = a_0$) by

$$\Omega_m(a) = \frac{\Omega_{m,0} H_0^2 a_0^3}{H^2 a^3}; \quad \Omega_\Lambda(a) = \frac{\Omega_{\Lambda,0} H_0^2}{H^2}. \quad (6)$$

In this paper we will consider only two cosmologies. The EdS case with $\Omega_m = 1$ and $\Omega_\Lambda = 0$ and the Λ CDM case with $\Omega_m = 0.29$ and $\Omega_\Lambda = 0.71$. The evolution of the ellipse is completely determined once six parameters are known: the three axes lengths $a_{i,init}$ and their velocities $\dot{a}_{i,init}$ at some initial epoch a_{init} .

³ Our notation differs slightly from BM96: $\alpha_i \equiv b_i$ and $\lambda_{ext,i} \equiv \lambda'_{ext,i}$ in BM96. With this, the two terms $\frac{\delta}{3} + \frac{\delta b'_i}{2}$ in BM96 are equal to $\frac{\delta \alpha_i}{2}$ in our notation.

⁴ A recent paper by Angrick & Bartelmann (2010) experimented with using a hybrid model to compute halo mass functions. They used the non-linear expression of BM96 at early times and reverted back to the linear expression of BM96 after turn-around. They concluded that the hybrid model and the non-linear model gave approximately the same results. We prefer to use a single function than a piecewise one so we stick to the BM96 form

An alternate description of the ellipse can be given by a set of nine *dimensionless* parameters

$$\lambda_{a,i} = 1 - \frac{a_i}{a} \quad (7a)$$

$$\lambda_{v,i} = \frac{1}{H} \frac{\dot{a}_i}{a_i} - 1 \quad (7b)$$

$$\lambda_{d,i} = \frac{\delta\alpha_i}{2} + \lambda_{ext,i}, \quad (7c)$$

where $i = 1, 2, 3$. The eigenvalues $\lambda_{d,i}$ are ordered as $\lambda_{d,1} \geq \lambda_{d,2} \geq \lambda_{d,3}$. This implies the ordering $\lambda_{v,1} \leq \lambda_{v,2} \leq \lambda_{v,3}$ and $\lambda_{a,1} \geq \lambda_{a,2} \geq \lambda_{a,3}$ at all times.

The three λ_a characterize the shape of the ellipse in terms of the deviation from the background. They correspond to the eigenvalues of the ‘comoving strain or deformation tensor’ (see Appendix A for definitions). Because the ellipsoid is always deformed along its principle axes, the deformation tensor is diagonal at all times. When an axis is collapsing $\lambda_a \rightarrow 1$, whereas for an expanding axes, $\lambda_a \rightarrow -\infty$.

The three λ_d correspond to the eigenvalues of the Hessian of peculiar gravitational field. Equation (7c) comprises of two terms; the first corresponds to the internal potential of the ellipse and the second to the external tidal field or the traceless gravitational tidal tensor. This definition and the fact that $\sum_i \alpha_i = 2$, implies

$$\delta = \lambda_{d,1} + \lambda_{d,2} + \lambda_{d,3}. \quad (8)$$

This is also the consistency condition arising from Poisson’s equation.

The three λ_v capture the deviation of the velocity of each axes from the background Hubble flow. They correspond to the eigenvalues of the tensor of (scaled) velocity derivatives. The trace part gives the ‘expansion’

$$\Theta = \frac{\nabla \cdot \mathbf{v}}{H} = \lambda_{v,1} + \lambda_{v,2} + \lambda_{v,3}. \quad (9)$$

where $\mathbf{v} = \dot{\mathbf{r}} - H\mathbf{r}$. In our definition, a negative λ_v implies a infall and a positive λ_v implies expansion. The three eigenvalues completely describe the curl-free velocity field of this model.

Not all λ s are independent. Equation (7c) defines an implicit relation between the three λ_d and the three λ_a . This can be seen by substituting eq. (8) in eq. (7c) and using the definitions of α_i and λ_a . In general, this relation is not linear. However, when the perturbations are small, the Zel’dovich approximation implies $\lambda_{a,i} = \lambda_{d,i}$ and $\lambda_{v,i} = -\lambda_{d,i}$. Equation (8) reduces to

$$\delta_{lin} = \lambda_{a,1} + \lambda_{a,2} + \lambda_{a,3}. \quad (10)$$

We emphasize that eq. (10) is not valid in the non-linear regime and we will illustrate the difference in §2.3. Usually it is standard to characterize the shape of the ellipse in terms of the ‘ellipticity’ e and ‘prolaticity’ p parameters (Bardeen et al. 1986). These are sometimes defined in terms of λ_d , but as has been emphasized in the literature (for e.g., Angrick & Bartelmann 2010), such definitions are valid in the linear regime. Connecting the shape to $\lambda_{d,i}$ in the non-linear regime necessarily involves solving for the three axes lengths.

An important assumption in the framework of Bond & Myers is that the principle axes of the deformation tensor and gravitational shear tensor coincide at all times during the evolution. If this assumption is violated then the ellipsoid can rotate and additional parameters need to be introduced to describe the dynamics. A more general framework that allows for rotation has been introduced by Eisenstein & Loeb (1995).

In terms of the λ parameters, the equations eq. (5) and its initial conditions are

$$\frac{d^2 \mathbf{a}}{da^2} + \left\{ \frac{1}{Ha} \frac{d}{da} (Ha) \right\} \cdot \frac{d\mathbf{a}}{da} = -\frac{3}{2a^2} \left[\Omega_m(a) \left\{ \frac{1}{3} + \lambda_d(a) \right\} - \frac{2}{3} \Omega_X(a) \right] \mathbf{a} \quad (11)$$

$$\mathbf{a}_{init} = a_{init} (1 - \lambda_{a,init}) \quad (12)$$

$$\left. \frac{d\mathbf{a}}{da} \right|_{a_{init}} = a_{init} (1 - \lambda_{a,init}) (1 - \lambda_{v,init}). \quad (13)$$

We have introduced boldface symbols for quantities that are 3-tuples. The product $(1 - \lambda_{a,init})(1 - \lambda_{v,init})$ *does not* denote a dot product. It is just the product of the corresponding components for each axes. The boldface \mathbf{a} denotes the axes of the ellipse and a denotes the scale factor of the background.

2.2 The Zel’dovich hyperplane

In general, the choice of $\lambda_{a,init}$ (or alternatively $\lambda_{d,init}$) and $\lambda_{v,init}$ are independent. However, for sufficiently early epochs, the Zel’dovich approximation (Zel’dovich 1970) is generally employed which states that the velocity is proportional to the acceleration. The proportionality constant is set by requiring ‘no growing modes’ (Buchert 1992; Susperregi & Buchert 1997). Physically, this means that there are no perturbations at the big bang epoch. At early epochs, when $\Omega_m \approx 1$, this gives the relation $\lambda_a = \lambda_d$ and $\lambda_v = -\lambda_d$. More generally, $\lambda_a = f(\Omega_m)\lambda_d$ and $\lambda_v = -f(\Omega_m)\lambda_d$, where $f(\Omega_m) = \Omega_m^{0.55}$ is the linear

growth rate $d \ln \delta / d \ln a$ (Linder 2005; we have ignored the weak Λ dependence). The linear density-velocity divergence is

$$\Theta_{lin} = -f(\Omega_m)\delta_{lin}. \quad (14)$$

This breaks down when the perturbations are in the non-linear regime. In spherical dynamics, the non-linear relation is given by the Zel'dovich curve (N13) which satisfies the form

$$\Theta_{sph} = \begin{cases} \frac{3}{2}\Omega_m^{\gamma_1} \left[1 - (1 + \delta_{sph})^{\frac{2}{3}\Omega_m^{\gamma_2}} \right] & -1 \leq \delta_{sph} < 1 \\ \Omega_m^{\gamma_1 + \gamma_2} \left[(1 + \delta_{sph})^{1/6} - (1 + \delta_{sph})^{1/2} \right] & \delta_{sph} \geq 1 \end{cases} \quad (15)$$

with $\gamma_1 = 0.56$ and $\gamma_2 = -0.01$ for a Λ CDM cosmology. This curve is time-invariant for an EdS cosmology, but changes for the Λ CDM case due to the variation of Ω_m throughout evolution. This formula is a combination of the forms of Bernardeau (1992) and Bilicki & Chodorowski (2008).

For triaxial dynamics, the situation is a bit more complicated because of higher dimensions, but the main idea remains the same. Density and velocity divergence are replaced by the 3D λ_d and λ_v and we wish to find the combination which ensures that there are no perturbations at the big bang. This set of 6-tuples defines a plane in the phase space of perturbations which we call the ‘Zel’dovich hyperplane’ and denote as $(\lambda_d, \lambda_v^{Zel})$. The superscript appears only on λ_v to denote the fact that λ_v is a function of λ_d . Computationally, λ_v^{Zel} is obtained as follows. Given the λ_d , first compute the λ_a from the implicit relation eq. (7c). This acts as a known initial condition for eq. (11). Then backward integrate eq. (11) with λ_v as a unknown initial value which is solved for three simultaneous conditions $\mathbf{a}(a=0) = 0$. It does not suffice to solve for only one or two of the axes. $\delta = 0$ at $a = 0$ only when all three axes are zero simultaneously. The value for a_{init} is taken to be the epoch for which the Zel’dovich plane is desired. For a EdS cosmology the 6-tuples (λ_d, λ_v) obtained this way are the same for all epochs, but they change with epoch for a Λ CDM cosmology. Unlike the spherical case, where the one-dimensional Zel’dovich curve could be easily visualized, it is not possible to visualize this 6D hyperspace for the triaxial case. But one can still numerically investigate the role played by the Zel’dovich hyperplane in the phase space evolution.

2.3 Dynamics in the phase space

In principle only six evolution equations are needed: one for each component of λ_d and λ_v . These are obtained by their definitions in eqs. (7a), (7b) and the evolution given by eq. (11). However, it turns out that the equation for $\lambda_{d,i}$ involves complicated functions of a_i which cannot be inverted easily since in the non-linear regime the relation between λ_d and the axes is implicit (see Appendix B). The system simplifies greatly if one adds the parameters λ_a to the set. Thus, the net system for the nine λ parameters is

$$\frac{d\lambda_{a,i}}{d \ln a} = -\lambda_{v,i}(1 - \lambda_{a,i}) \quad (16a)$$

$$\frac{d\lambda_{v,i}}{d \ln a} = -\frac{1}{2} [3\Omega_m(a)\lambda_{d,i} - \{\Omega_m(a) - 2\Omega_\Lambda(a) - 2\}\lambda_{v,i} + 2\lambda_{v,i}^2] \quad (16b)$$

$$\frac{d\lambda_{d,i}}{d \ln a} = -(1 + \delta) \left(\delta + \frac{5}{2} \right)^{-1} \left(\lambda_{d,i} + \frac{5}{6} \right) \sum_{j=1}^3 \lambda_{v,j} \quad (16c)$$

$$+ \left(\lambda_{d,i} + \frac{5}{6} \right) \sum_{i=1}^3 (1 + \lambda_{v,i}) - \left(\delta + \frac{5}{2} \right) (1 + \lambda_{v,i}) \\ + \sum_{j \neq i} \frac{\{\lambda_{d,j} - \lambda_{d,i}\} \cdot \{(1 - \lambda_{a,i})^2(1 + \lambda_{v,i}) - (1 - \lambda_{a,j})^2(1 + \lambda_{v,j})\}}{(1 - \lambda_{a,i})^2 - (1 - \lambda_{a,j})^2},$$

where

$$\delta = \sum_{i=1}^3 \lambda_{d,i}.$$

One can check that this system reduces to eq. (15) when all three axes are equal and gives the expected linear relation when the λ s are small (see Appendix B). For the EdS case, this system forms an autonomous set of equations i.e., the r.h.s. is independent of the variable ‘ a ’ where as for the Λ CDM case it is a non-autonomous system i.e., explicit appearance of the dependent variable a in the r.h.s. This is related to the fact that the Zel’dovich hyperplane is time-invariant in the EdS case, but not for Λ CDM.

The relevance of the Zel’dovich hyperplane can be understood by following the trajectory of an initial point $(\lambda_{d,init}, \lambda_{v,init})$ and examining how much this trajectory deviates from the Zel’dovich hyperplane at late times. Start with a set of random initial conditions at $a = 0.001$ drawn from the probability distribution function given by Doroshkevich (1970) (see Rossi 2012

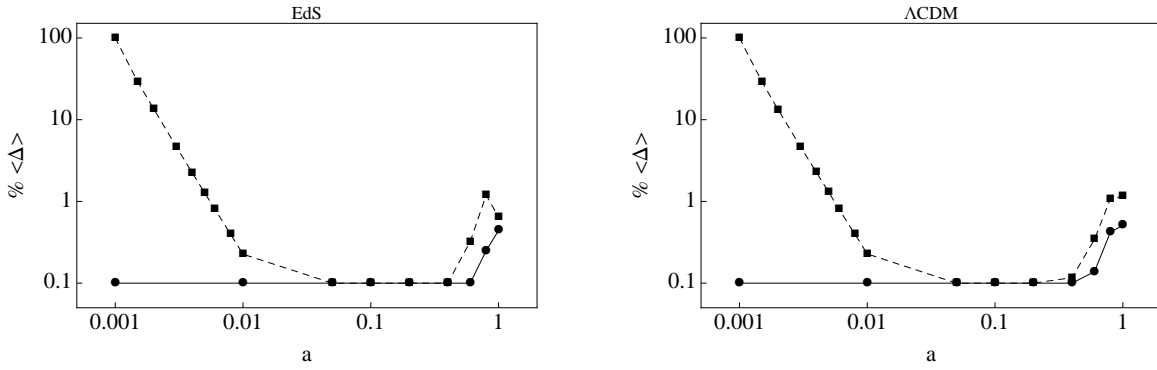


Figure 1. The attracting nature of the Zel’dovich hyperplane: the solid (dashed) lines correspond to $\lambda_{v,init} = -\lambda_{d,init}$ ($\lambda_{v,init} = -2\lambda_{d,init}$). The latter set has a 100% deviation at the initial time $a = 0.001$. The deviation decreases exponentially with a as $\sim a^{-2.6}$ for both EdS and Λ CDM cosmologies.

and Angrick 2013 for recent extensions)

$$p(\lambda_{d,1}, \lambda_{d,2}, \lambda_{d,3}) = \frac{15^3}{8\pi\sqrt{5}\sigma^6} \exp\left(-\frac{3I_1^2}{\sigma^2} + \frac{15I_2}{2\sigma^2}\right), \quad (17)$$

where $\sigma \equiv \sigma(R_f)$, the r.m.s. fluctuation at the scale R_f , $I_1 = \lambda_{d,1} + \lambda_{d,2} + \lambda_{d,3}$ and $I_2 = \lambda_{d,1}\lambda_{d,2} + \lambda_{d,2}\lambda_{d,3} + \lambda_{d,1}\lambda_{d,3}$. This PDF gives the value at $a = 1$; the value at $a = 0.001$ is obtained by multiplying by the appropriate linear growth factor $D_+(a) = 5\Omega_{m,0}/2 \int_0^a [a'H(a')/H_0]^{-3} da$ (Dodson 2003). Each point is evolved according to eqs. (16a) to (16c). At a future epoch, a point on this trajectory is a 6-tuple denoted by $\{\lambda_d^{evol}, \lambda_v^{evol}\}$. For this λ_d^{evol} compute the corresponding Zel’dovich λ_v^{Zel} as described in section §2.2. This gives the corresponding point on the Zel’dovich hyperplane denoted as $\{\lambda_d^{evol}, \lambda_v^{Zel}\}$. The distance between the two points in the 6D space is a measure of how close the trajectory gets to the Zel’dovich hyperplane. We define the relative deviation at any epoch as

$$\Delta(a) = \frac{\|\lambda_v^{evol}(a) - \lambda_v^{Zel}(a)\|}{\|\lambda_v^{Zel}(a)\|}, \quad (18)$$

where, $\|\mathbf{x} - \mathbf{y}\|$ denotes the norm $\sqrt{\sum_i (x_i - y_i)^2}$.

Figure 1 shows the average relative deviation as a function of a for the EdS (left panel) and Λ CDM models (right). For each case, two sets of initial conditions were considered. The first set was initialized at $a = 0.001$ using the standard Zel’dovich approximation: $\lambda_{v,init} = -\lambda_{d,init}$ (solid line). The error between this linear limit and the exact values that lie along the Zel’dovich hyperplane was found to be 0.1%. This value was set as a measure of the tolerance i.e. at any other epoch, the error was chosen to be the maximum of two numbers: mean deviation (average over 50 points) and the tolerance. It was found that at most future epochs, the error stays within 0.1% rising at late epochs, but staying within 1%. The second set of initial conditions (dashed line) was started with $\lambda_{v,init} = -2\lambda_{d,init}$ corresponding to 100% deviation at $a = 0.001$. This case clearly illustrates the attracting nature of the Zel’dovich hyperplane. The relative deviation quickly drops down from 100% at $a = 0.001$ to the sub percent level at $a = 0.1$. This implies that even trajectories that start far off from the Zel’dovich hyperplane eventually find their way onto it. For this set of initial conditions too, the error rises slightly near $a \sim 1$.

The reason for this late time rise is not yet fully clear. Some understanding can be gained by looking at it from the point of Lagrangian perturbation theory (LPT). In the most general formalism, the first order LPT solution consists of three terms: one corresponding to the initial acceleration field and other two corresponding to the longitudinal and transverse parts of the initial velocity field (Buchert 1992). An important assumption in the construction is that the initial fields all contribute at first order. The time dependent coefficients of these terms have both growing and decaying modes. The higher order spatial solutions all get fixed once the initial density and velocity fields are fixed. In general, every higher order term has a decaying mode. The Zel’dovich approximation is a special case, which assumes that, initially, the transverse component of the velocity is zero (for good physical reasons) and the longitudinal component is proportional to the acceleration field, with the constant determined by demanding ‘no decaying modes’. This assumption implies that there are no decaying modes in the first order solution, but these modes will be present in higher order solutions. Imposing ‘no perturbations at the big bang’ is equivalent to imposing ‘no decaying modes’ at every order in the LPT solution. This requires adding more spatial terms at second order which can be interpreted to give a ‘higher order’ contribution to the initial velocity field. Including these terms, can generate additional growing modes (see Ehlers & Buchert 1997; Nadkarni-Ghosh & Chernoff 2013 for the LPT series construction). Thus, the two solutions, one obtained by imposing ‘no growing modes’ initially and then evolving and the other obtained by imposing ‘no growing modes at every order’ are different and the differences could potentially grow at late times. Whether this explains the observed behaviour quantitatively is yet to be understood and is beyond the scope of this paper. Here, it

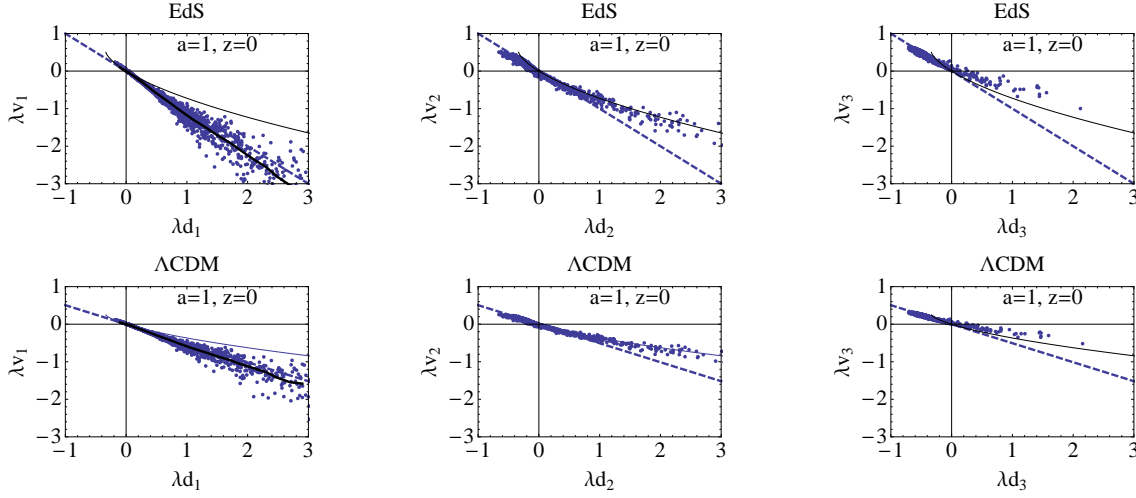


Figure 2. Snapshot at $a = 1$ of the 2D $\lambda_d - \lambda_v$ slices of the 6D Zel'dovich hyperplane. The solid line is the Zel'dovich curve for the sphere given by eq. (15) and the dashed line is the linear relation $\lambda_v = -\lambda_d$. The first panel corresponds to the largest eigenvalues. The 'mean' relation between them is very close to the linear relation.

suffices to note that the differences are of the order of 1% and we conclude that to this accuracy, the Zel'dovich hyperplane does indeed play a special role in the dynamics.

The entire Zel'dovich hyperplane cannot be visualized directly. Nevertheless, it helps to visualize 2D subspaces defined by the parameters $(\lambda_{d,i}, \lambda_{v,i})$. Figure 2 shows the three such projections at $a = 1$. In each plot, the dotted line shows the linear relation $\lambda_{v,i} = -f(\Omega_m)\lambda_{d,i}$. The solid curved line is the Zel'dovich curve based on spherical collapse eq. (15); in this case, $\lambda_d = \frac{\delta_{sph}}{3}$ and $\lambda_v = \frac{\Theta_{sph}}{3}$, where δ_{sph} and Θ_{sph} are given by eq. (15). The main interesting point observed here is that the 'mean' relation between the largest eigenvalue $\lambda_{d,1}$ and the corresponding $\lambda_{v,1}$ is close to the linear one. It is clear that in the non-linear regime, each axes has a different relation between λ_d and λ_v i.e., the 'vectors' $\boldsymbol{\lambda}_d$ and $\boldsymbol{\lambda}_v$ are no longer proportional. This means that although in the triaxial model, the gravitational shear tensor and velocity derivative tensor always have the same principle axes, their eigenvalues are not simple multiples of each other. This is related to the fact that the gravitational acceleration and peculiar velocity are not parallel to each other in the non-linear regime, which has been discussed earlier in the context of Lagrangian perturbation theory (for e.g., Bagla & Padmanabhan 1996; Susperregi & Buchert 1997; Nadkarni-Ghosh & Chernoff 2013). We also note the distinction between the breakdown of parallelism and breakdown of proportionality; for e.g. for the sphere with a radially dependent overdensity, the acceleration and velocity in the non-linear regime are always parallel at any point (both are radial), but yet as fields they are not proportional.

2.4 δ vs. trace of the deformation tensor

Using the phase space evolution one can also investigate the relation between the exact non-linear density $\delta = \sum_i \lambda_{d,i}$ and its linear approximation $\delta_l = \sum_i \lambda_{a,i}$. Figure 3 shows the difference at three epochs: $a = 0.01, 0.4$ and 1 . The dashed line denotes the linear relation and the solid line denotes the relation when all the axes are equal. In this case, $\lambda_a = \delta_{l,sph}/3$, where $\delta_{l,sph}$ is the linear spherical overdensity and from eqs. (1) and (7a) we have

$$\delta_{sph} = \frac{1}{(1 - \frac{\delta_{l,sph}}{3})^3} - 1. \quad (19)$$

The dots indicate the numerically evolved data points. It is clear that at early times the linear approximation is valid, but at later epochs (middle and right panels), it fails for values as low as $\delta_l \sim 0.01$, which are small enough to be considered linear. For example, for some points with $\delta_l = 0.01$, the middle panel ($a = 0.4$) shows the non-linear δ to be 10 times higher. The right panel ($a = 1$) shows it to be 100 times higher. Thus, the linear approximation severely underestimates the actual value of δ and in particular ceases to be valid at late times even for linear densities.

This discrepancy can be understood if one examines the mathematical expressions relating δ and δ_l . From eqs. (1) and (7a)

$$\delta = \prod_{i=1}^3 (1 - \lambda_{a,i})^{-1} \quad (20)$$

$$\approx \delta_l + \sum_{i=1}^3 \lambda_{a,i}^2 + \lambda_{a,1}\lambda_{a,2} + \lambda_{a,2}\lambda_{a,3} + \lambda_{a,1}\lambda_{a,3} + \mathcal{O}(\lambda^3) \quad (21)$$

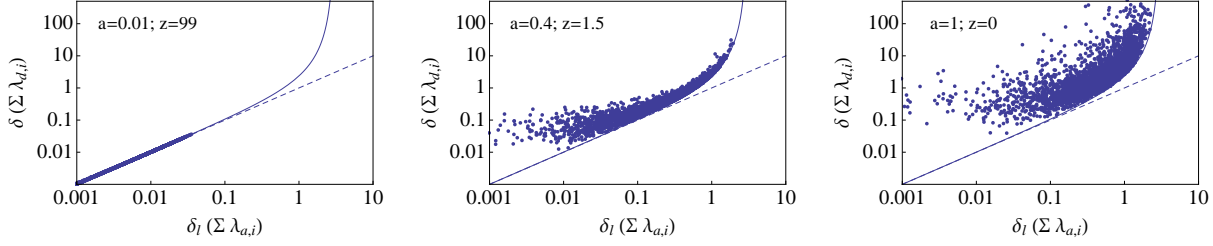


Figure 3. Difference between the exact δ given by $\sum_i \lambda_{a,i}$ and the sum of the eigenvalues of the strain tensor which is used as an approximation. In the linear regime they agree $\sum_{i=1} \lambda_{a,i}$, but deviate at late times.

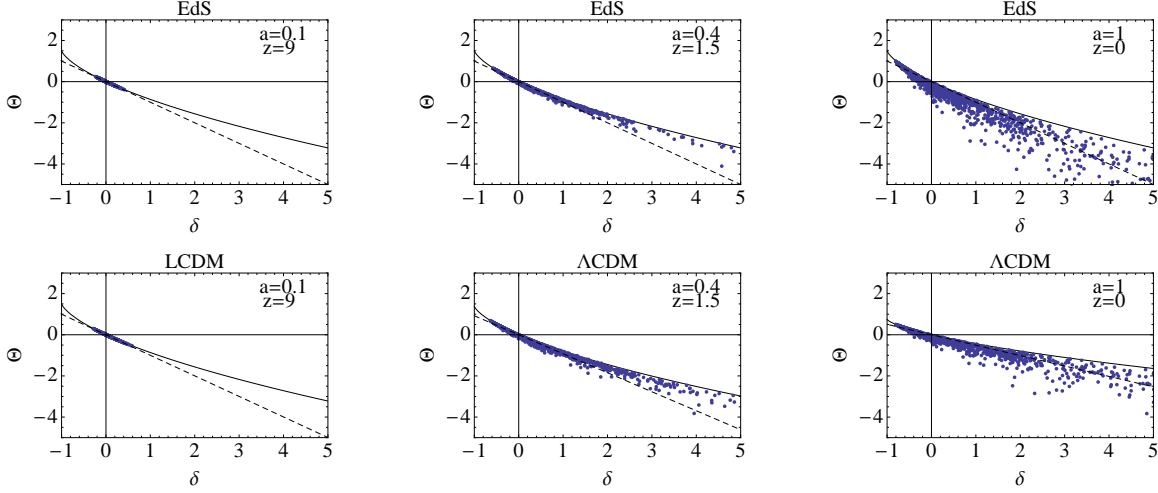


Figure 4. The non-linear $\delta - \Theta$ relation based on triaxial dynamics. The dashed line is the linear relation and the solid line is the Zel'dovich curve eq. (15). At early epochs, both the sphere and ellipsoid obey linear dynamics. Velocity shear effects induce a scatter for the triaxial dynamics.

At early times, all λ_a s are small and the second order correction is small for all values of λ_a . However, due to the asymmetry, it is possible to have two values of λ_a large ($\sim \mathcal{O}(1)$) but with opposite signs. This asymmetry is already present in the initial conditions. The initial PDF given by eq. (17) has only 16% probability of generating all λ s with the same sign (all positive or all negative). In 84% of the cases, there are atleast two with different signs (this distribution stays more or less constant through the evolution; see Appendix C). Suppose $\lambda_{a,1} = -\lambda_{a,3} \sim \mathcal{O}(1)$ and $\lambda_{a,2}$ is small. Then the second order term reduces to $\lambda_{a,1}^2 \sim \mathcal{O}(1)$, i.e. not small compared to the first order terms. To illustrate this, we consider one sample point in the right panel. This has values $\{\delta_l, \delta\} = \{0.004, 1.134\}$ and the individual $\lambda_a = \{0.708, -0.819, 0.115\}$. The second order terms in this case add up to 0.5, much larger than the linear value. Therefore, strictly speaking, the approximation that $\delta \sim \sum_{i=1}^3 \lambda_{a,i}$ is valid only at very early epochs $a \lesssim 0.01$.

In passing, we also note that all the data points lie above the solid curve which represents the spherical relation. This can be proven mathematically: for a fixed sum $\sum_i \lambda_{a,i}$, the l.h.s. of eq. (20) is minimum when all the axes are equal.

3 DYNAMICS IN THE $\delta - \Theta$ PLANE.

In this section we analyse the dynamics in the 2D space corresponding to the variables $\delta = \sum \lambda_{a,i}$ and $\Theta = \sum \lambda_{v,i}$.

3.1 Ellipsoid vs. sphere

The dynamical equations for the variables δ and Θ are given by

$$\frac{d\delta}{d \ln a} = -(1 + \delta)\Theta \quad (22a)$$

$$\frac{d\Theta}{d \ln a} = -\frac{1}{2} [3\Omega_m(a)\delta - \{\Omega_m(a) - 2\Omega_\Lambda(a) - 2\}\Theta + 2\Theta^2 - 4\lambda_{v,1}\lambda_{v,2} - 4\lambda_{v,1}\lambda_{v,3} - 4\lambda_{v,2}\lambda_{v,3}]. \quad (22b)$$

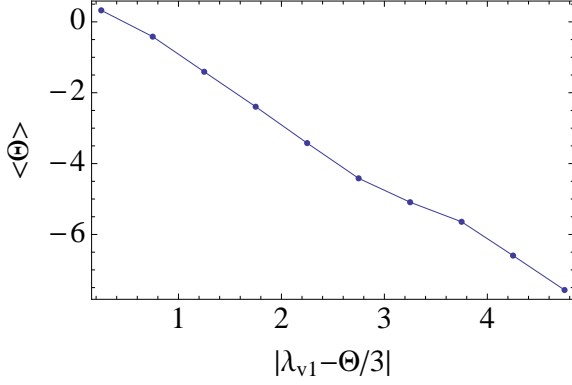


Figure 5. Mean Θ at a point vs. the magnitude of largest eigenvalue of the shear tensor $|\lambda_{v1} - \Theta/3|$ at that point. The relation of the scatter to the shear part of the velocity derivative tensor is clear. For large negative values of Θ the shear is high and decreases as we go to the void limit.

The δ equation follows from the definitions in eqs. (1), (7b) and (9). The Θ equation follows from summing eq. (16b) over all i and rearranging the terms. Figure 4 shows $\{\delta, \Theta\}$ pairs from one realization of the case $\sigma_G = 1$. The dashed line is the prediction of linear theory given in eq. (14). The solid black line is the Zel'dovich curve of the sphere and it acts as a limiting case for the dynamics. The corresponding equations for the sphere are (N13)

$$\frac{d\delta_{sph}}{d \ln a} = -(1 + \delta)\Theta \quad (23a)$$

$$\frac{d\Theta_{sph}}{d \ln a} = -\frac{1}{2} \left[3\Omega_m(a)\delta - \{\Omega_m(a) - 2\Omega_\Lambda(a) - 2\} \Theta + \frac{2}{3}\Theta^2 \right]. \quad (23b)$$

For a given δ , Θ is smaller for the ellipse as compared to the sphere. Mathematically, this can be seen by computing the rate of evolution $d\Theta/d\delta$:

$$\left. \frac{d\Theta}{d\delta} \right|_{ell} - \left. \frac{d\Theta}{d\delta} \right|_{sph} = \frac{1}{2} \frac{N(\lambda_{v,1}, \lambda_{v,2}, \lambda_{v,3})}{(1 + \delta)\Theta}. \quad (24)$$

where the numerator $N(\lambda_{v,1}, \lambda_{v,2}, \lambda_{v,3}) = 4 \left(\frac{\Theta^2}{3} - \lambda_{v,1}\lambda_{v,2} - \lambda_{v,1}\lambda_{v,3} - \lambda_{v,2}\lambda_{v,3} \right)$. The terms $(1 + \delta)$ and $N(\lambda_{v,1}, \lambda_{v,2}, \lambda_{v,3})$ are both positive (see Appendix D). Thus, when $\Theta < 0$, i.e., the region is contracting, $\frac{d\Theta}{d\delta}_{ell} < \frac{d\Theta}{d\delta}_{sph}$ and when Θ is positive $\frac{d\Theta}{d\delta}_{ell} > \frac{d\Theta}{d\delta}_{sph}$. Since $\frac{d\Theta}{d\delta}$ is always negative these inequalities imply that triaxiality causes overdense regions to infall faster and underdense regions to expand slower. Triaxiality also implies some regions which are underdense but infalling, a possibility excluded in the spherical model.

Unlike the sphere, the $\delta - \Theta$ relation now has a spread. The spread is least at the void limit $\delta = -1$ and increases as $\delta \rightarrow \infty$. This means that the void limit of the ellipse is the same as the sphere and we can compute it analytically. From eq. (15) this is

$$\Theta_{max} = \Theta|_{\delta=-1} = \frac{3}{2} \Omega_m^{0.56}. \quad (25)$$

The exponent of Ω_m is slightly different from the value of 0.6 given in Bernardeau et al. (1997); Bernardeau (1992). There have been proposals to constrain the value of Ω_m using this value of maximal expansion in voids (for e.g.: Dekel & Rees 1994; Bernardeau et al. 1997).

3.2 Scatter in the $\delta - \Theta$ plane

The non-linear density-velocity divergence relation (DVDR), also known as the gravity-velocity relation, has been discussed in great detail by various authors in the past (Bernardeau 1992; Nusser et al. 1991; Gramann 1993; Bernardeau & van de Weygaert 1996; Chodorowski & Lokas 1997; Chodorowski et al. 1998; Bernardeau et al. 1999; Kudlicki et al. 2000; Cieliegi et al. 2003; Kitaura et al. 2012). These analyses are based on higher order perturbation theory, either in Eulerian or Lagrangian frame, or on numerical simulations. All of them show a scatter around the mean-relation which is usually attributed to two reasons. One reason is the non-locality of the dynamics captured by higher order perturbation theory. In linear theory, both in Eulerian space (continuity equation) or in Lagrangian space (Zel'dovich approximation), the DVDR relation is local i.e., the velocity divergence/velocity at a point is given by the density/gravitational acceleration at that point. Higher orders of perturbation theory depend on derivatives of lower orders and to determine them, the field needs to be known everywhere (non-local). This non-locality makes the relation stochastic or non-deterministic because although the field equations are deterministic, the initial conditions are random. Another related reason is the traceless ‘shear’ component of the tensor of

velocity derivatives. The eigenvalues of this tensor are $\lambda_{v,i} - \Theta/3$ and their relation to the scatter has been discussed by Chodorowski (1997) from the point of view of perturbation theory. The triaxial model provides a nice illustration of the same effect based on local dynamics. This is clear from considering eq. (24). The terms that differ from the sphere are all second order and vanish when all the axes are equal. Figure 5 illustrates this effect for the data plotted in figure 4. The mean Θ is plotted as a function of the largest eigenvalue of the shear tensor ($\lambda_{v,1} - \Theta/3$). In the void limit when $\Theta > 0$, the shear is small and increases in the overdense regions as Θ becomes more negative. The scatter shows the same trend. In other words, the scatter arises from the asymmetry in the system. Indeed, the non-linear DVDR based on the spherical collapse model, which is both local and symmetric, and shows no scatter.

In simulations (for e.g., Bernardeau, Chodorowski, Lokas, Stompor, & Kudlicki 1999; Kudlicki, Chodorowski, Plewa, & Ryczka 2000) it is seen that the ‘mean $\delta - \Theta$ relation’ is given by Bernardeau’s formula based on second order perturbation theory Bernardeau (1992). This formula is a reasonably good fit to the Zel’dovich curve, implying that spherical dynamics approximately acts as a mean description. On the other hand, triaxial collapse predicts that the scatter is bounded by the Zel’dovich curve, in disagreement with simulations. This disagreement is not surprising - simulations solve for the dynamics almost exactly. Effects such as rotation of the halo and non-local physics due to interaction between the environment are all accounted for, where as, the triaxial model considered here is a rather simplistic, rotation-less, local model. Ohta, Kayo, & Taruya (2003), whose work was based on the ellipsoidal collapse model also observed this kind of sharp cut-off at the spherical limit. Here we are able to explain it based on the ellipsoidal equations and the ensuing phase space dynamics.

4 MARGINAL PROBABILITIES $p(\Theta)$ AND $p(\delta)$.

As an application of this method, we compute the marginal probabilities $p(\Theta)$ and $p(\delta)$ and qualitatively discuss the joint PDF $p(\delta, \Theta)$.

4.1 Numerical runs

The numerical runs were performed by evolving a set of 10^4 initial conditions using the equations of phase space dynamics given in eq. (16). At the desired final time the δ and Θ are computed according to definitions given in eqs. (8) and (9). Each set was drawn from the distribution given by eq. (17). Three scales were considered: $\sigma_G = 0.5, 1$ and 2 . The initial σ_G is related to the scale of the perturbation: the exact dependence depends on the shape and amplitude of the power-spectrum. For the BBKS power spectrum with $n_s = 1$ and $\sigma_8 = 0.9$, $\sigma_G = 0.5, 1, 2$ corresponds to length scales of $R_f = 16.4, 7$ and $3.65 h^{-1}\text{Mpc}$ respectively. Two cosmologies were considered: EdS ($\Omega_m = 1, \Omega_\Lambda = 0$) and ΛCDM ($\Omega_m = 0.29, \Omega_\Lambda = 0.71$). The realization at $a = 1$ was the same for the two cosmologies, but the values at the initial epoch $a = 0.001$ were set by multiplying by the correct growth rate factor. By $a = 1$ roughly one-tenth of the points had undergone collapse. For each σ value, five realizations were evolved; the PDF is the average over five and the error bars correspond to the standard deviation.

4.2 Theoretical Estimates for comparison

The one-point distributions of the non-linear density and velocity fields have been discussed in great detail in the past. One of the most popular forms for the density PDF is the empirically motivated log-normal model given by Coles & Jones (1991). While this form has been checked by simulations (for e.g., Kayo, Taruya, & Suto 2001, Kitaura et al. 2012), there are others based on more analytical approaches. For example, Kofman et al. (1994) constructed the non-linear PDF from the linear Gaussian PDF by expressing the non-linear density as a function of the linear λ_d via the Zel’dovich approximation. Further work by Bernardeau & collaborators (Bernardeau 1994; Kofman et al. 1994) gave forms for the large scale density PDF, both in Eulerian and Lagrangian spaces, from cumulants calculated using perturbation theory. Later Fosfalba & Gaztanaga (1998a) gave an alternative approach to computing the cumulants using the spherical collapse model as a local approximation for the dynamics. Ohta, Kayo, & Taruya (2003, 2004) formulated the differential equations for the evolution of the one-point PDFs and solved them using the spherical and ellipsoidal collapse as local approximations for the dynamics. More recently, Lam & Sheth (2008a,b) derived the density PDF both in real space and redshift space based on excursion sets and ellipsoidal collapse.

The PDFs that come from the present analysis are in the Eulerian frame. We found that the log-normal form, which is probably the simplest of the ones above, did not match well in the highly overdense and void regions. The perturbative form proposed by Bernardeau (1994) (henceforth B94) promises to do better in these regions. Hence the final PDF we chose for

comparison is combination of the two:

$$p(\delta) = \begin{cases} p_{B94}^{void}(\delta) & -1 \leq \delta < -0.4 \\ p_{L-N}(\delta) & -0.4 \leq \delta < 1 \\ p_{B94}^{high}(\delta) & \delta \geq 1, \end{cases} \quad (26)$$

where

$$p_{B94}^{void}(\delta)d\delta = \left(\frac{7 - 5(1 + \delta)^{2/3}}{4\pi\sigma_\delta^2} \right)^{1/2} (1 + \delta)^{-5/3} \times \exp \left[-\frac{9}{8\sigma_\delta^2} \left(-1 + \frac{1}{(1 + \delta)^{2/3}} \right)^2 \right] d\delta \quad (27)$$

$$p_{L-N}(\delta)d\delta = \frac{1}{\sqrt{2\pi}(1 + \delta)\sigma_{ln}} \times \exp \left[-\frac{\{\log(1 + \delta) + \sigma_{ln}^2/2\}^2}{2\sigma_{ln}^2} \right] d\delta \quad (28)$$

$$p_{B94}^{high}(\delta)d\delta = f_c \frac{3a_{s\delta}\sigma_\delta}{4\sqrt{\pi}} (1 + \delta)^{-5/2} \times \exp \left[-\frac{|y_{s\delta}|\delta + |\phi_{s\delta}|}{\sigma_\delta^2} \right] d\delta \quad (29)$$

with $\sigma_{ln} = \ln(1 + \sigma_\delta^2)$, $a_{s\delta} = 1.84$, $y_{s\delta} = -0.184$, $\phi_{s\delta} = -0.03$. We have chosen the $n = -3$ values for the parameters a_s, y_s, ϕ_s from B94 (this corresponds to the case of no smoothing). σ_δ^2 is the variance at the relevant epoch and is related to the linear variance today through $\sigma_\delta^2(a) = \sigma_G^2 D_+^2(a)/D_+^2(a=1)$. The correction factor $f_c = [1 + 2(0.8 - \sigma_\delta)\sigma_\delta^{-1.3}(1 + \delta)^{-0.5}]$ was introduced by B94 to account for the fact that the PDF calculated by the perturbative form did not perform well at high δ .

For the velocity divergence the form for $p(\Theta)$ proposed in B94

$$p(\Theta) = \begin{cases} p_{B94}^{void}(\Theta) & 1.5 \geq \Theta \geq -0.5 \\ p_{B94}(\Theta) & \Theta < -0.5 \end{cases} \quad (30)$$

where

$$p_{B94}^{void}(\Theta)d\Theta = \frac{1}{3}(3 + 2\tau)^2 \sqrt{\frac{1 + 2\tau}{3\pi\sigma_\Theta^2(3 + 2\tau)}} \times \exp \left(-\frac{\tau^2}{2\sigma_\Theta^2} \right) d\Theta; \quad \tau = \Theta \left(1 - \frac{3}{2}\Theta \right)^{-1} \quad (31)$$

$$p_{B94}^{high}(\Theta)d\Theta = f_c \frac{3a_{s\Theta}\sigma_\Theta}{4\sqrt{\pi}} \left(\frac{3}{2} - \Theta \right)^{-5/2} \times \exp \left[\frac{|y_{s\Theta}|\Theta + |\phi_{s\Theta}|}{\sigma_\Theta^2} \right] d\Theta \quad (32)$$

with $a_{s\Theta} = 1.67$, $y_{s\Theta} = -0.222$, $\phi_{s\Theta} = -0.042$. The PDF for the Λ CDM cosmology is given by rescaling $p_{\Lambda CDM}(\Theta) = p_{EdS}(\Theta \rightarrow \Theta/f(\Omega_m))$, where the σ_Θ is the variance of the scaled variable. The correction factor $f_c = [1 + 30(0.8 - \sigma_\Theta)\sigma_\Theta^{-1.3}(1.5 - \Theta)^{-0.5}]$ was introduced in B94 to account for the fact that the expression eq. (32) underestimates the exact answer. It was used only for the cases $\sigma_G = 2$, $a = 0.4, 1$ and $\sigma_G = 1$, $a = 1$. For all other cases, $f_c = 1$.

These ‘patched’ up PDFs are not normalized. Our aim is not to provide a precise normalized PDF but rather to use these forms as a comparison so as to understand and illustrate the potential and limitation of this method.

4.3 Results: $p(\delta)$ and $p(\Theta)$

We construct PDFs from the data generated by the numerical runs described in §4.1. The output is analysed at three different epochs: $a = 0.05, 0.4$ and 1 (corresponding to $z = 19, 1.5$ and 0). Three scales were considered: $\sigma_G = 0.5$ (red), 1 (blue dotted), 2 (brown, dashed).

Figure 6 shows the marginal probability distribution $p(\delta)$ at the three epochs. The points denote the data and the lines denotes the analytic distribution. The top and bottom panels are the EdS and Λ CDM cosmologies. At early times, the departure from Gaussianity is small and the log-normal model provides a good fit. At later epochs, the void regions continue to fit well with the Bernardeau form, but the high density regions show a deviation between numerics and analytical approximations, even with the correction factor of B94 included. This departure can be attributed to two reasons. Firstly, triaxial collapse is local, whereas higher order perturbation theory can account for non-local effects. The other reason is be that the perturbative approximation fails at high values of δ and the correction factors given in B94 are expected to work only for $\sigma_\delta \lesssim 1$. Nevertheless, the reasonably good agreement for voids is encouraging. It means that the triaxial collapse model can be used effectively to model voids.

The PDF of Θ , shown in figure 7 shows a similar behaviour. The x -axis in this case is $\Theta_{max} - \Theta$, where Θ_{max} is the maximal value in voids given by eq. (25). The point Θ_{max} in this variable corresponds to $\Theta = 0$ and is shown on the graph. Points to the left of Θ_{max} correspond to voids and those to the right correspond to overdensities. We see that the analytic expressions given by eq. (30) fit very well at early times when the perturbations are in the linear regime. At later epochs, the agreement is maintained in the void regions, but gets worse in the overdense regions.

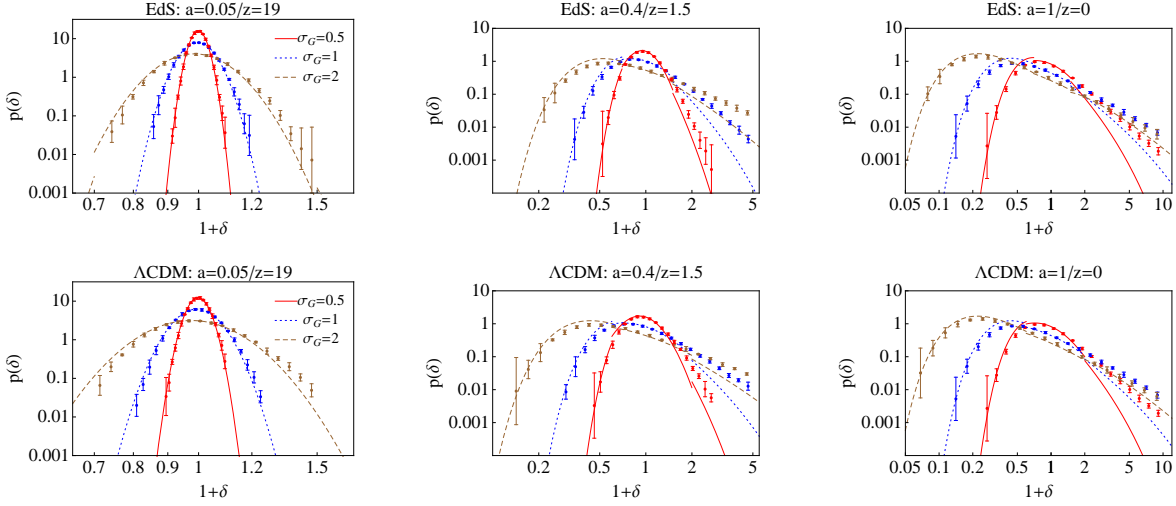


Figure 6. Evolution of $p(\delta)$ vs $1 + \delta$ for three values of σ_G for the EdS and Λ CDM models. Agreement with the theoretical forms given in eq. (26) is better in the void regions than in the high density tails.

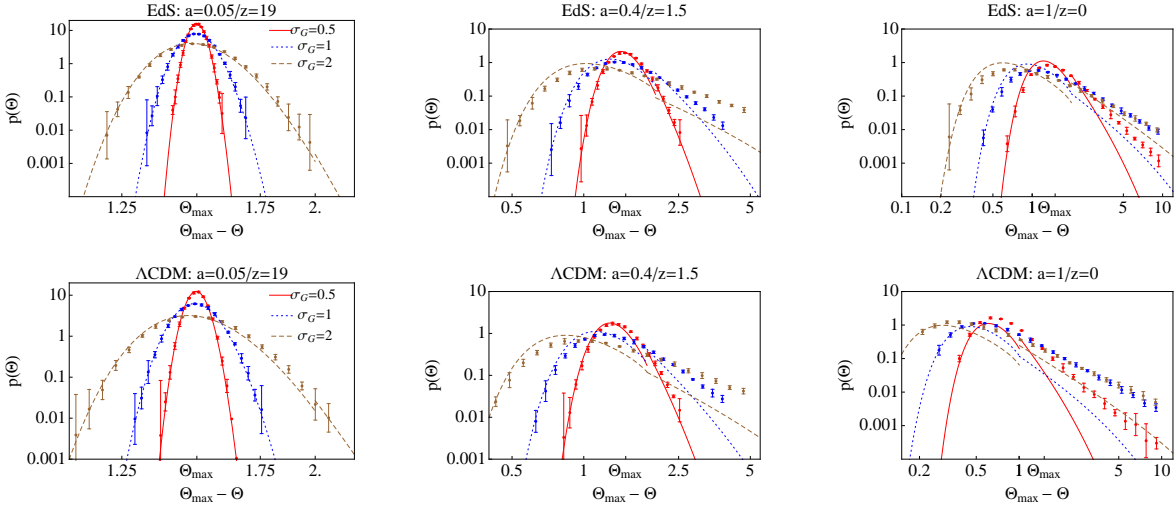


Figure 7. Evolution of $p(\Theta)$ vs $\Theta_{max} - \Theta$, where $\Theta_{max} = 1.5\Omega_m^{0.56}$. For EdS, Θ_{max} is constant with time, whereas for Λ CDM it changes. Agreement with the theoretical forms of B94 given in eq. (30) is maintained in voids throughout the evolution, but worsens in the overdense regions $\Theta_{max} - \Theta \gg 1$.

4.4 Joint pdf

Figure 8 shows the evolution of the joint PDF $p(\delta, \Theta)$ for the EdS model (left panel) and the Λ CDM model (right panel) at $a = 1$. The region above the Zel'dovich curve is overlaid to indicate the sharp cut-off observed in figure 4. Our graphs are in reasonably good agreement with the joint PDF plotted by Otha *et al* (figure 5), which was also based on ellipsoidal collapse, although they have a slight spill over which may possibly be a plotting artifact. Both for EdS and Λ CDM, the scatter increases as time elapses (at early times the scatter is minimal; all points obey the local linear relation). However, the limiting spherical curve in the two cases is different. The scatter is greater for a higher σ_G (not shown). In N13, it was demonstrated how the attracting nature of the Zel'dovich curve could be exploited to remove parameter degeneracies related to the power spectrum normalization or index. But the same cannot be done with the joint PDF. Unlike the spherical Zel'dovich curve which does not depend on the initial σ_G , the joint PDF carries the signature of the initial width (we investigated two more values of σ_G ; data not shown).

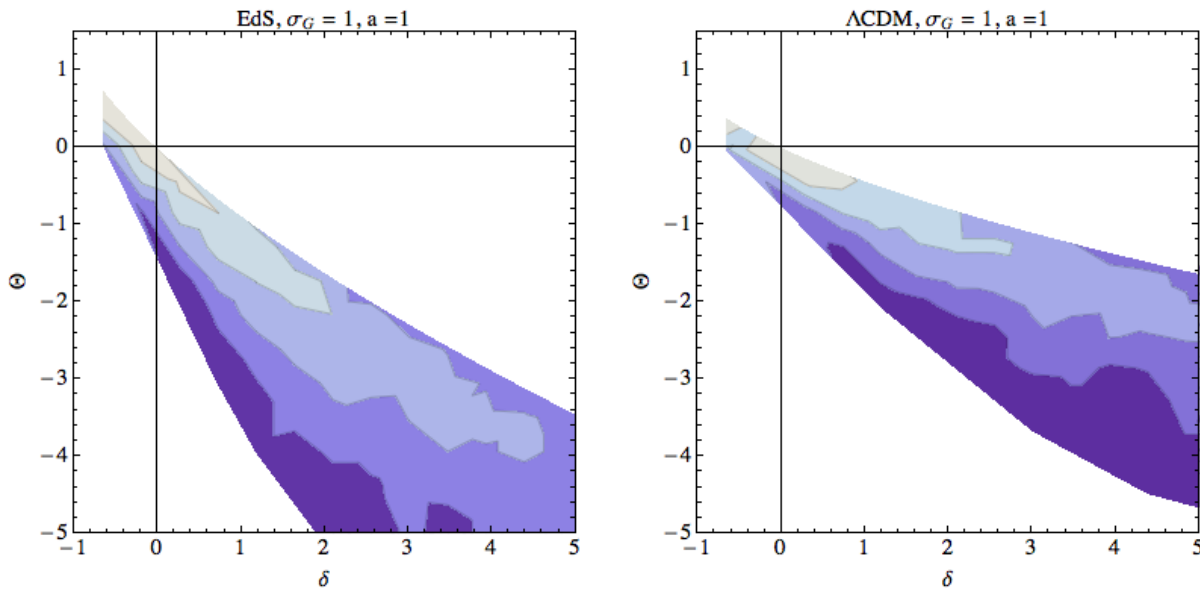


Figure 8. The joint PDF $p(\delta, \theta)$. The Zel’dovich relation forms a limiting case for the joint PDF. The spread is related to the shear component of the velocity field as was discussed in §3.2

5 CONCLUSION

The main points of this paper can be summarized as follows.

- We recast the well-known Bond & Myers’ set of equations governing the axes evolution of a triaxial system into a new set (eq. (16)) for nine dimensionless parameters: $\lambda_{a,i}$, $\lambda_{v,i}$ and $\lambda_{d,i}$, $i=1,2,3$. These correspond to eigenvalues of the deformation tensor, the tensor of velocity derivatives and the tensor of second derivatives of the gravitational potential. The main advantage of this reform is that it eliminates the dependence on complicated elliptic integrals which are present in the original system. Furthermore, it allows one to track the eigenvalues directly giving more insight into the dynamics. With these definitions $\delta = \sum \lambda_{d,i}$ and the scaled velocity divergence $\Theta = \sum \lambda_{v,i}$.

- In linear theory ‘no decaying modes’ implies that the λ_d and λ_v for each axis are proportional, but this breaks down in the non-linear regime. Using the ideas in N13, we extended this to the non-linear regime by imposing the condition ‘no perturbations at the big bang’. This gives a relation between the three λ_d and λ_v s at any epoch and this set of 6-tuples lies on a hyperplane in 6D. This was termed the ‘Zel’dovich hyperplane’ in analogy with the Zel’dovich curve in the spherical case. This plays a special role in the dynamics of perturbations. Perturbations, no matter where they start in phase space, eventually lie along this plane within an error of 1%. In particular, we find that along this plane, in the highly non-linear regime, the mean relation between the largest value of λ_d and the corresponding λ_v stays close to linear.

- Using the same phase space equations, we analysed the relation between the density δ and the trace of the deformation tensor $\sum \lambda_{a,i}$. In the linear regime, $\lambda_{d,i} \approx \lambda_{a,i}$ and $\delta \approx \sum \lambda_{a,i}$. To understand the validity of this statement we examined the $\delta - \sum \lambda_{a,i}$ relation a function of time. We find that linearity of this relation breaks down at late times even for ‘linear’ δ values. This emphasizes the point that the ‘linearity’ refers to the individual λ s. In the non-linear regime, because of a cancellation between λ s of opposite signs, it is possible to have a ‘linear’ δ although the λ s are of order unity.

- One of the aims of this paper was to understand the $\delta - \Theta$ relation in the non-linear regime. From the nine-dimensional set for the eigenvalues, we obtained a two dimensional set that governs the $\delta - \Theta$ dynamics. Unlike the linear or spherical relation, the triaxial system shows a scatter. This scatter arises from the ‘shear’ part of the velocity derivative tensor as was shown earlier by Chodorowski (1997) using higher order perturbation theory. The triaxial collapse provides a nice illustration of the same based on ‘local’ dynamics. The nature of the scatter is fundamentally different than that observed in simulations. Triaxial collapse predicts that the spherical relation acts as an upper bound to the scatter, where as simulations (for e.g. Bernardeau, Chodorowski, Lokas, Stompor, & Kudlicki 1999) predict it to be closer to the mean. This discrepancy can probably attributed to effects of rotation, interaction between the neighbours etc. that are captured by simulations, but ignored in the simple model considered here.

- As an application of this method, we examined the pdf of the density and velocity perturbations. We focussed primarily on the marginal PDFs $p(\Theta)$ and $p(\delta)$ and discussed the joint PDF only qualitatively. We compared them to known analytic forms in the literature and found that the agreement was rather good in the void regions, suggesting that even this simple

model may be useful to describe realistic void dynamics. The mis-match in the high density tails of the PDFs is probably due to a combination of the breakdown of the model as well as the analytic form which is based on perturbation theory. As another application we will consider the evolution of axis ratios (paper II, in preparation Nadkarni-Ghosh & Singhal 2014).

In N13, we showed how the attracting nature of the Zel'dovich curve could be exploited to remove certain parameter degeneracies related to the normalization or slope of the initial power spectrum. Trying to exploit the same feature in the Zel'dovich hyperplane is not so straightforward. One has to find some relation between the three λ_d and λ_v which does not show a scatter and depends only on the background cosmology. This is left to future work.

There are many limitations of the triaxial model considered here. The first important assumption is that the principle axes stay fixed throughout the evolution i.e., no rotations are included. Second, the ellipse is isolated; the dynamics is local. There are no interactions between neighbours. The effect of the environment is modeled through the effective external non-linear tidal tensor, which depends completely on the axes lengths. The first extension of this analysis would be to follow the more complete set of equations such as those given by Eisenstein & Loeb (1995), which includes rotation. Additional parameters will be required to model the rotational degree of freedom, but the basic language in terms of dimensionless parameters remains the same. Building more sophisticated analytic models could help address some of the issues related to alignment or initial shapes of haloes which have been raised in recent simulations (see for e.g. Despali, Tormen, & Sheth 2013, Hoffman et al. 2012). This work presents the first step towards such a goal.

6 ACKNOWLEDGEMENTS

We would like to thank Sagar Chakraborty for useful discussions regarding dynamical systems. S.N. would like to thank the hospitality of ICTP, Trieste, and discussions with Pierluigi Monaco and Ravi Sheth which sowed the seeds of this work.

REFERENCES

- Angrick C., 2013, ArXiv e-prints, 1305, 497
- Angrick C., Bartelmann M., 2010, *Astronomy and Astrophysics*, 518, 38
- Bagla J. S., Padmanabhan T., 1996, *The Astrophysical Journal*, 469, 470
- Bardeen J. M., Bond J. R., Kaiser N., Szalay A. S., 1986, *The Astrophysical Journal*, 304, 15
- Bernardeau F., 1992, *The Astrophysical Journal*, 390, L61
- Bernardeau F., 1994, *Astronomy and Astrophysics*, 291, 697
- Bernardeau F., Chodorowski M. J., Lokas E. L., Stompor R., Kudlicki A., 1999, *Monthly Notices of the Royal Astronomical Society*, 309, 543
- Bernardeau F., van de Weygaert R., 1996, *Monthly Notices of the Royal Astronomical Society*, 279, 693
- Bernardeau F., van de Weygaert R., Hivon E., Bouchet F. R., 1997, *Monthly Notices of the Royal Astronomical Society*, 290, 566
- Bilicki M., Chodorowski M. J., 2008, *Monthly Notices of the Royal Astronomical Society*, 391, 1796
- Bond J. R., Myers S. T., 1996, *Astrophysical Journal Supplement Series*, 103, 1
- Buchert T., 1992, *Monthly Notices of the Royal Astronomical Society*, 254, 729737
- Carlson B., 1987, *Mathematics of Computation*, 49, 595
- Carlson B., 1989, *Mathematics of Computation*, 53, 327
- Chodorowski M. J., 1997, *Monthly Notices of the Royal Astronomical Society*, 292, 695
- Chodorowski M. J., Lokas E. L., 1997, *Monthly Notices of the Royal Astronomical Society*, 287, 591
- Chodorowski M. J., Lokas E. L., Pollo A., Nusser A., 1998, *Monthly Notices of the Royal Astronomical Society*, 300, 1027
- Cieciegel P., Chodorowski M. J., Kiraga M., Strauss M. A., Kudlicki A., Bouchet F. R., 2003, *Monthly Notices of the Royal Astronomical Society*, 339, 641
- Coles P., Jones B., 1991, *Monthly Notices of the Royal Astronomical Society*, 248, 1
- Dekel A., Rees M. J., 1994, *The Astrophysical Journal Letters*, 422, L1
- Despali G., Tormen G., Sheth R. K., 2013, *Monthly Notices of the Royal Astronomical Society*, 431, 1143
- Dodelson S., 2003, *Modern Cosmology*. Academic Press, Elsevier
- Doroshkevich A. G., 1970, *Astrophysics*, 6, 320
- Ehlers J., Buchert T., 1997, *General Relativity and Gravitation*, 29, 733764
- Eisenstein D. J., Loeb A., 1995, *The Astrophysical Journal*, 439, 520
- Fosalba P., Gaztanaga E., 1998a, *Monthly Notices of the Royal Astronomical Society*, 301, 503
- Fosalba P., Gaztanaga E., 1998b, *Monthly Notices of the Royal Astronomical Society*, 301, 535
- Gramann M., 1993, *The Astrophysical Journal Letters*, 405, L47
- Gunn J. E., Gott, III J. R., 1972, *The Astrophysical Journal*, 176, 1
- Hoffman Y., Metuki O., Yepes G., Gottlber S., Forero-Romero J. E., Libeskind N. I., Knebe A., 2012, *Monthly Notices of the Royal Astronomical Society*, 425, 2049
- Icke V., 1973, *Astronomy and Astrophysics*, 27, 1
- Jing Y. P., Suto Y., 2002, *The Astrophysical Journal*, 574, 538
- Kayo I., Taruya A., Suto Y., 2001, *The Astrophysical Journal*, 561, 22
- Kitaura F.-S., Angulo R. E., Hoffman Y., Gottlber S., 2012, *Monthly Notices of the Royal Astronomical Society*, 425, 2422
- Kofman L., Bertschinger E., Gelb J. M., Nusser A., Dekel A., 1994, *The Astrophysical Journal*, 420, 44
- Kudlicki A., Chodorowski M., Plewa T., Ryczka M., 2000, *Monthly Notices of the Royal Astronomical Society*, 316, 464
- Lam T. Y., Sheth R. K., 2008a, *Monthly Notices of the Royal Astronomical Society*, 389, 1249
- Lam T. Y., Sheth R. K., 2008b, *Monthly Notices of the Royal Astronomical Society*, 386, 407
- Lin C. C., Mestel L., Shu F. H., 1965, *The Astrophysical Journal*, 142, 1431
- Linder E. V., 2005, *Physical Review D*, 72, 43529
- Lynden-Bell D., 1964, *The Astrophysical Journal*, 139, 1195
- Matarrese S., Pietroni M., 2007, *Journal of Cosmology and Astro-Particle Physics*, 06, 026
- Matsubara T., 2008, *Physical Review D*, 77, 63530
- Monaco P., 1995, *The Astrophysical Journal*, 447, 23
- Monaco P., Sefusatti E., Borgani S., Crocce M., Fosalba P., Sheth R. K., Theuns T., 2013, *Monthly Notices of the Royal Astronomical Society*, 433, 2389
- Nadkarni-Ghosh S., 2013, *Monthly Notices of the Royal Astronomical Society*, 428, 1166
- Nadkarni-Ghosh S., Chernoff D. F., 2011, *Monthly Notices of the Royal Astronomical Society*, 410, 1454
- Nadkarni-Ghosh S., Chernoff D. F., 2013, *Monthly Notices of the Royal Astronomical Society*, 431, 799
- Nadkarni-Ghosh S., Singhal A., 2014, In Preparation
- Nusser A., Dekel A., Bertschinger E., Blumenthal G. R., 1991, *The Astrophysical Journal*, 379, 6

- Ohta Y., Kayo I., Taruya A., 2003, *The Astrophysical Journal*, 589, 1
 Ohta Y., Kayo I., Taruya A., 2004, *The Astrophysical Journal*, 608, 647
 Peebles P., 1980, *The Large-Scale Structure of the Universe* (pages 63-65). Princeton University Press
 Press W., Teukolsky S., Vetterling W., Flannery B., 2002, *Numerical Recipes in C++*. Cambridge University Press
 Press W. H., Schechter P., 1974, *Astrophysical Journal*, 187, 425438
 Rossi G., 2012, *Monthly Notices of the Royal Astronomical Society*, 421, 296
 Scherrer R. J., Gaztanaga E., 2001, *Monthly Notices of the Royal Astronomical Society*, 328, 257
 Sheth R. K., Mo H. J., Tormen G., 2001, *Monthly Notices of the Royal Astronomical Society*, 323, 1
 Susperregi M., Buchert T., 1997, *Astronomy and Astrophysics*, 323, 295
 White S. D. M., Silk J., 1979, *Astrophysical Journal*, 231, 19
 Zel'dovich Y. B., 1970, *Astronomy and Astrophysics*, 5, 84

APPENDIX A: DEFINITIONS OF THE TENSORS

The physical and comoving axes of the ellipse are

$$r_i = a_i q_i \quad x_i = \frac{a_i}{a} q_i, \quad (\text{A1})$$

where q_i is the initial Lagrangian coordinate of the i -th axis. Initially, the a_i are different from a , so q_i is not the initial comoving coordinate. If we want to characterize the deformation from the sphere then for the sphere $q_1 = q_2 = q_3$. The deformation and velocity are

$$s_i = q_i - x_i = \left(1 - \frac{a_i}{a}\right) q_i \quad (\text{A2})$$

$$v_i = \dot{r}_i - H r_i = \left(\frac{\dot{a}_i}{a_i} - H\right) r_i. \quad (\text{A3})$$

The deformation tensor is

$$e_{ij} = \frac{1}{2} \left(\frac{\partial s_i}{\partial q_j} + \frac{\partial s_j}{\partial q_i} \right) = \lambda_{a,i} \delta_{ij}. \quad (\text{A4})$$

Note that we differ from BM96 by a minus sign. However, their relevant eigenvalues (denoted as $\lambda_{v,A}$) are negative of the eigenvalues of their e_{ij} . We have expressed it so that the λ_a are eigenvalues of e_{ij} . This is just a matter of convention. The important point is that in both conventions $\lambda_a = \lambda_d$ in the linear regime and $\sum \lambda_{a,i} = \delta$. The tensor of velocity derivatives is

$$\frac{1}{2H} \left(\frac{\partial v_i}{\partial r_j} + \frac{\partial v_j}{\partial r_i} \right) = \lambda_{v,i} \delta_{ij}. \quad (\text{A5})$$

The gravitational potential ϕ_p (scaled by $4\pi G \bar{\rho}_m$) for the ellipsoid is

$$\phi_p = \frac{1}{2} \sum_i \lambda_{d,i} r_i^2. \quad (\text{A6})$$

The Hessian of the gravitational potential is

$$\frac{\partial^2 \phi_p}{\partial r_i \partial r_j} = \lambda_{d,i} \delta_{ij}. \quad (\text{A7})$$

The peculiar gravitational acceleration is $\ddot{r} = \nabla \phi_p$. Comparing with eq. (2) one can ensure that the definition is consistent.

APPENDIX B: DERIVATION OF THE PHASE SPACE EQUATIONS

With the definitions of the parameters the equation for the axes evolution takes the form

$$\frac{\ddot{a}_i}{a_i} = -\frac{H^2}{2} \left(\Omega_m \left\{ \frac{1}{3} + \lambda_{d,i} \right\} - \frac{2}{3} \Omega_\Lambda \right). \quad (\text{B1})$$

Ω_m and Ω_Λ are functions of a .

(i) Evolution of $\lambda_{a,i}$: from the definition $\lambda_{a,i} = 1 - \frac{a_i}{a}$, it follows that

$$\dot{\lambda}_{a,i} = -\left(\frac{\dot{a}_i}{a} - \frac{a_i}{a} H \right). \quad (\text{B2})$$

But from the definition of $\lambda_{v,i}$, $\dot{a}_i = H a_i (1 + \lambda_{v,i})$. Substituting in the above equation, using the definition of $\lambda_{a,i}$ and converting from derivatives w.r.t. time to derivatives w.r.t. $\ln a$ gives

$$\frac{d\lambda_{a,i}}{d \ln a} = -\lambda_{v,i} (1 - \lambda_{a,i}). \quad (\text{B3})$$

(ii) Evolution of $\lambda_{v,i}$: from the definition $\lambda_{v,i} = \frac{1}{H} \frac{\dot{a}_i}{a_i}$, we have

$$\dot{\lambda}_{v,i} = \frac{\dot{a}_i}{a_i} \left(1 - \frac{1}{H^2} \frac{\ddot{a}}{a} \right) + \frac{1}{H} \left(\frac{\ddot{a}_i}{a_i} - \frac{\dot{a}_i^2}{a_i^2} \right). \quad (\text{B4})$$

Using eq. (B1), the background evolution $\frac{\ddot{a}}{a} = -\frac{H^2}{2}(\Omega_m - 2\Omega_\Lambda)$ and the definitions λ_v gives

$$\frac{d\lambda_{v,i}}{d \ln a} = -\frac{3}{2}\Omega_m \lambda_{d,i} + \lambda_{v,i} \left(-1 + \frac{\Omega_m}{2} - \Omega_\Lambda \right) - \lambda_{v,i}^2. \quad (\text{B5})$$

(iii) Evolution of $\lambda_{d,i}$: $\lambda_{d,i}$ is defined as

$$\lambda_{d,i} = \frac{\delta \alpha_i}{2} + \frac{5}{4} \left(\alpha_i - \frac{2}{3} \right), \quad (\text{B6})$$

where

$$\delta = \frac{a^3}{a_1 a_2 a_3} - 1, \quad (\text{B7})$$

$$\alpha_i = a_1 a_2 a_3 f_i \quad (\text{B8})$$

$$\text{and } f_i = \int_0^\infty d\tau (a_i^2 + \tau)^{-\frac{3}{2}} \prod_{j=1}^3 (a_j^2 + \tau)^{-\frac{1}{2}}. \quad (\text{B9})$$

Hence,

$$\frac{d\lambda_{d,i}}{dt} = \left(\frac{\delta}{2} + \frac{5}{4} \right) \frac{d\alpha_i}{dt} + \frac{\alpha_i}{2} \frac{d\delta}{dt}. \quad (\text{B10})$$

From the definitions,

$$\frac{d\delta}{dt} = -H(1 + \delta) \sum_i \lambda_{v,i} \quad (\text{B11})$$

$$\frac{d\alpha_i}{dt} = H\alpha_i \sum_{i=1}^3 (1 + \lambda_{v,i}) + a_1 a_2 a_3 \frac{df_i}{dt}. \quad (\text{B12})$$

The non-trivial part is the term $\frac{df_i}{dt}$. We proceed to evaluate it. Consider the case $i = 1$.

$$\frac{df_1}{dt} = 2a_1 \dot{a}_1 \int_0^\infty d\tau \left(-\frac{3}{2}(a_1^2 + \tau)^{-\frac{5}{2}}(a_2^2 + \tau)^{-\frac{1}{2}}(a_3^2 + \tau)^{-\frac{1}{2}} \right) - a_2 \dot{a}_2 I_3 - a_3 \dot{a}_3 I_2, \quad (\text{B13})$$

where

$$I_3 = \int_0^\infty d\tau (a_1^2 + \tau)^{-\frac{3}{2}} (a_2^2 + \tau)^{-\frac{3}{2}} (a_3^2 + \tau)^{-\frac{1}{2}} \quad (\text{B14})$$

and I_2 is obtained by interchanging 2 and 3 in I_3 . Rewrite $-\frac{3}{2}(a_1^2 + \tau)^{-\frac{5}{2}}$ in the first integrand as $\frac{d(a_1^2 + \tau)^{-\frac{3}{2}}}{d\tau}$ and integrate by parts to give

$$\frac{df_1}{dt} = -\frac{2}{a_1 a_2 a_3} \frac{\dot{a}_1}{a_1} + (a_1 \dot{a}_1 - a_2 \dot{a}_2) I_3 + (a_1 \dot{a}_1 - a_2 \dot{a}_2) I_2 \quad (\text{B15})$$

The solutions for the integrals I_2 and I_3 can be found in a paper by Carlson (1987); equation 2.10. These expressions give the integrals I_2 and I_3 in terms of $R_F(a_1^2, a_2^2, a_3^2)$.

$$I_3 = \frac{1}{(a_1^2 - a_2^2)^2} \left(\frac{2}{3}(2a_3^2 - a_1^2 - a_2^2) R_D(a_1^2, a_2^2, a_3^2) - 4R_F(a_3^2, a_1^2, a_2^2) + \frac{a_1^2 + a_2^2}{a_1 a_2 a_3} \right) \quad (\text{B16})$$

But from relations in Carlson (1989), specifically, equations 2.12, 2.17 and 2.26, it can be shown that

$$3R_F(a_1^2, a_2^2, a_3^2) = a_1^2 R_D(a_2^2, a_3^2, a_1^2) + a_2^2 R_D(a_3^2, a_1^2, a_2^2) + a_3^2 R_D(a_1^2, a_2^2, a_3^2) \quad (\text{B17})$$

where

$$R_D(a_2^2, a_3^2, a_1^2) = \frac{3}{2} \frac{\alpha_1}{a_1 a_2 a_3}, \quad R_D(a_3^2, a_1^2, a_2^2) = \frac{3}{2} \frac{\alpha_2}{a_1 a_2 a_3} \quad \text{etc} \quad (\text{B18})$$

Using the two above results from Carlson's paper and the relation $\sum_i \alpha_i = 2$, gives

$$a_1 a_2 a_3 \frac{df_1}{dt} = -2 \frac{\dot{a}_1}{a_1} + \frac{(\alpha_2 - \alpha_1)(a_1 \dot{a}_1 - a_2 \dot{a}_2)}{a_1^2 - a_2^2} + \frac{(\alpha_3 - \alpha_1)(a_1 \dot{a}_1 - a_3 \dot{a}_3)}{a_1^2 - a_3^2} \quad (\text{B19})$$

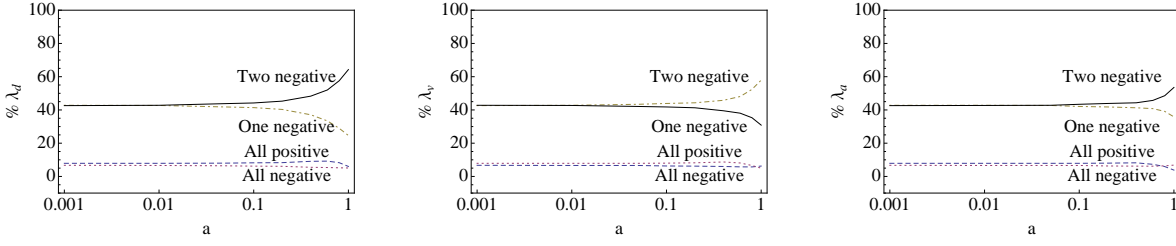


Figure C1. The evolution of the signs of the individual λ parameters. The initial pdf has a distribution of 42% for two eigenvalues λ_d positive or two negative. At early times this is the same for λ_v and λ_a . We find that for all three λ parameters, this distribution evolves in a similar manner changing only slightly at later epochs near $a = 1$.

Using eqs. (B10), (B11), (B12) and (B19) along with the definitions of λ_v and λ_d gives

$$\begin{aligned} \frac{d\lambda_{d,i}}{d\ln a} &= -(1+\delta) \left(\delta + \frac{5}{2} \right)^{-1} \left(\lambda_{d,i} + \frac{5}{6} \right) \sum_{j=1}^3 \lambda_{v,j} \\ &+ \left(\lambda_{d,i} + \frac{5}{6} \right) \sum_{i=1}^3 (1 + \lambda_{v,i}) - \left(\delta + \frac{5}{2} \right) (1 + \lambda_{v,i}) \\ &+ \sum_{j \neq i} \frac{\{\lambda_{d,j} - \lambda_{d,i}\} \cdot \{(1 - \lambda_{a,i})^2 (1 + \lambda_{v,i}) - (1 - \lambda_{a,j})^2 (1 + \lambda_{v,j})\}}{(1 - \lambda_{a,i})^2 - (1 - \lambda_{a,j})^2}. \end{aligned} \quad (\text{B20})$$

Note that only the equation for λ_v depends on the background cosmology. The equations for λ_a and λ_d stay unchanged.

Spherical and linear limits: When all three axes are equal, $\lambda_d = \delta_{sph}/3$ and $\lambda_v = \Theta_{sph}/3$. It is easy to check that the λ_v equation reduces to eq. (23b) for the sphere. For case of the λ_d equation, the last term can be shown to be tending to zero by substituting $\lambda_j = \lambda_i + \epsilon$ and taking the limit $\epsilon \rightarrow 0$. The second and third terms cancel and we are left with the first which reduces to eq. (23a). Linearizing the λ_v and λ_d equations gives $d\lambda_{d,i}/d\ln a = -\lambda_{v,i}$ and $d\lambda_{v,i}/d\ln a = \lambda_{v,i}$ giving the correct linear limit $d\lambda_{v,i}/d\lambda_{d,i} = -1$.

APPENDIX C: EVOLUTION OF THE SIGNS OF THE λ PARAMETERS

The distribution of the signs of the λ parameters stays more or less constant throughout the evolution. This distribution may potentially change for initial conditions that are non-Gaussian.

APPENDIX D: POSITIVITY OF $N(\lambda_{v,1}, \lambda_{v,2}, \lambda_{v,3})$

$$N(\lambda_{v,1}, \lambda_{v,2}, \lambda_{v,3}) = \frac{4(\lambda_{v,1} + \lambda_{v,2} + \lambda_{v,3})^2}{3} - 4\lambda_{v,1}\lambda_{v,2} - 4\lambda_{v,2}\lambda_{v,3} - 4\lambda_{v,1}\lambda_{v,3} \quad (\text{D1})$$

$$= \frac{4}{3} [\lambda_{v,1}^2 + \lambda_{v,2}^2 + \lambda_{v,3}^2 - \lambda_{v,1}\lambda_{v,2} - \lambda_{v,2}\lambda_{v,3} - \lambda_{v,1}\lambda_{v,3}]. \quad (\text{D2})$$

We want to prove that for any three numbers a, b and c , $a^2 + b^2 + c^2 - ab - bc - ac > 0$.

Proof: Write $a^2 + b^2 + c^2 - ab - bc - ac = c(c-b) + b(b-a) + a(a-c)$. Without loss of generality, let $a \leq b \leq c$. This implies that $b-a \geq 0$ and $c-b \geq 0$. Note that

$$c(c-b) + b(b-a) \geq b(c-b) + b(b-a) = b(c-a) \geq a(c-a). \quad (\text{D3})$$

The first relation follows because $c \geq b$ and the third because $b \geq a$ and $c-a \geq 0$. Therefore,

$$c(c-b) + b(b-a) + a(a-c) \geq 0 \quad (\text{D4})$$

and hence $N \geq 0$.